Science Advances
AAAS

advances.sciencemag.org/cgi/content/full/7/1/eabe1386/DC1

Supplementary Materials for

Recessive *NOS1AP* variants impair actin remodeling and cause glomerulopathy in humans and mice

Amar J. Majmundar, Florian Buerger, Thomas A. Forbes, Verena Klämbt, Ronen Schneider, Konstantin Deutsch, Thomas M. Kitzler, Sara E. Howden, Michelle Scurr, Ker Sin Tan, Mickaël Krzeminski, Eugen Widmeier, Daniela A. Braun, Ethan Lai, Ihsan Ullah, Ali Amar, Amy Kolb, Kaitlyn Eddy, Chin Heng Chen, Daanya Salmanullah, Rufeng Dai, Makiko Nakayama, Isabel Ottlewski, Caroline M. Kolvenbach, Ana C. Onuchic-Whitford, Youying Mao, Nina Mann, Marwa M. Nabhan, Seymour Rosen, Julie D. Forman-Kay, Neveen A. Soliman, Andreas Heilos, Renate Kain, Christoph Aufricht, Shrikant Mane, Richard P. Lifton, Shirlee Shril, Melissa H. Little, Friedhelm Hildebrandt*

*Corresponding author. Email: friedhelm.hildebrandt@childrens.harvard.edu

Published 1 January 2021, *Sci. Adv.* **7**, eabe1386 (2021)
DOI: 10.1126/sciadv.abe1386

The PDF file includes:

Figs. S1 to S10

Other Supplementary Material for this manuscript includes the following:

(available at advances.sciencemag.org/cgi/content/full/7/1/eabe1386/DC1)

Movies S1 and S2

Established Pathway
[ref. literature]

Human Podocyte

Novel NS Pathway
(data from current study)

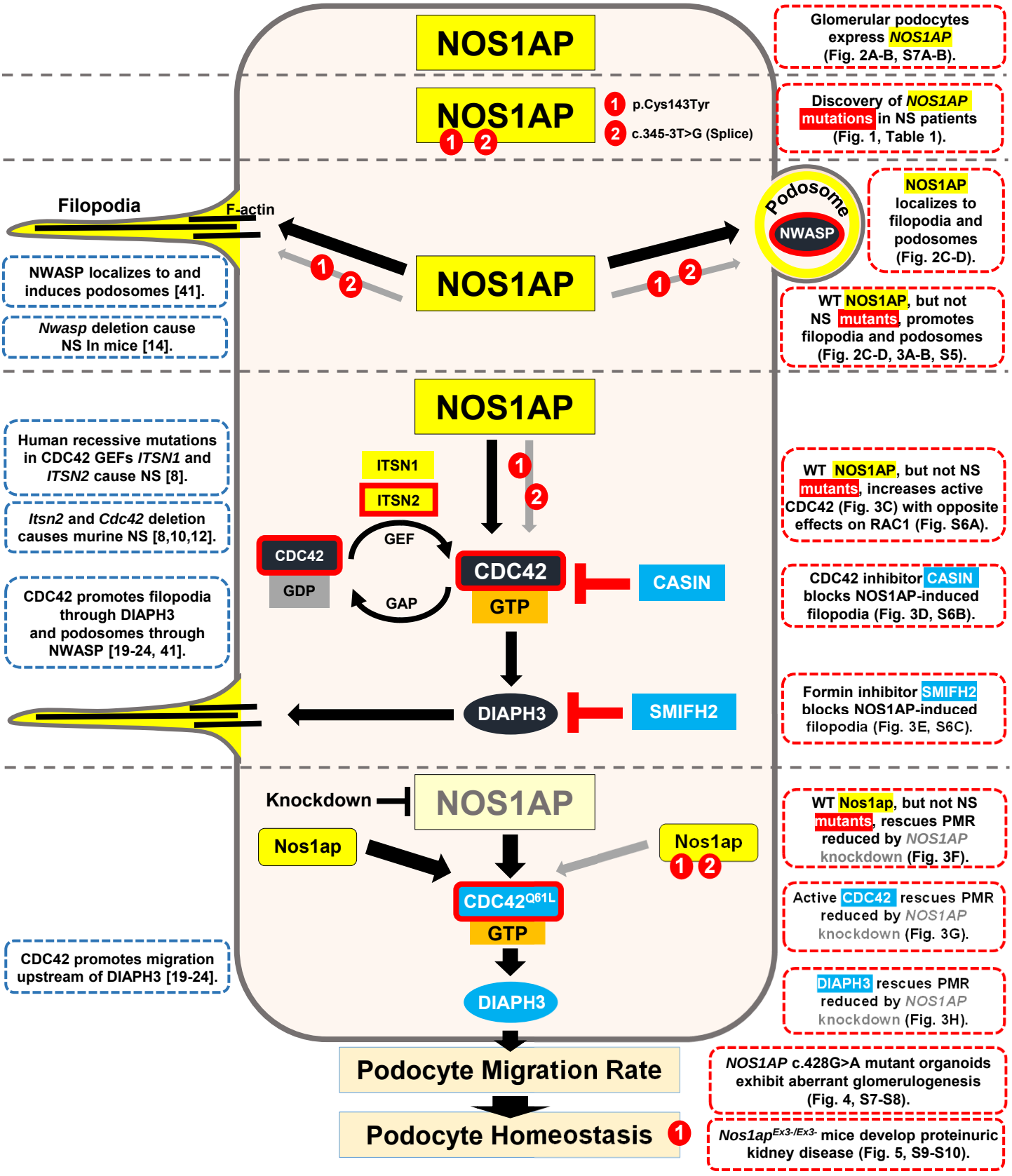

Glomerular podocytes express *NOS1AP* (Fig. 2A-B, S7A-B).

Discovery of *NOS1AP* mutations in NS patients (Fig. 1, Table 1).

NOS1AP localizes to filopodia and podosomes (Fig. 2C-D).

WT NOS1AP, but not NS mutants, promotes filopodia and podosomes (Fig. 2C-D, 3A-B, S5).

NWASP localizes to and induces podosomes [41].

Nwasp deletion cause NS In mice [14].

Human recessive mutations in CDC42 GEFs *ITSN1* and *ITSN2* cause NS [8].

Itsn2 and *Cdc42* deletion causes murine NS [8,10,12].

CDC42 promotes filopodia through DIAPH3 and podosomes through NWASP [19-24, 41].

WT NOS1AP, but not NS mutants, increases active CDC42 (Fig. 3C) with opposite effects on RAC1 (Fig. S6A).

CDC42 inhibitor CASIN blocks NOS1AP-induced filopodia (Fig. 3D, S6B).

Formin inhibitor SMIFH2 blocks NOS1AP-induced filopodia (Fig. 3E, S6C).

WT Nos1ap, but not NS mutants, rescues PMR reduced by *NOS1AP* knockdown (Fig. 3F).

Active CDC42 rescues PMR reduced by *NOS1AP* knockdown (Fig. 3G).

DIAPH3 rescues PMR reduced by *NOS1AP* knockdown (Fig. 3H).

CDC42 promotes migration upstream of DIAPH3 [19-24].

NOS1AP c.428G>A mutant organoids exhibit aberrant glomerulogenesis (Fig. 4, S7-S8).

Nos1ap$^{Ex3-/Ex3-}$ mice develop proteinuric kidney disease (Fig. 5, S9-S10).

Figure S1. *NOS1AP* mutations impair the CDC42 actin regulatory pathway in nephrotic syndrome.

This diagram delineates the functional aspects of *NOS1AP* loss-of-function symbolized in a human podocyte. We identified recessive mutations in *NOS1AP* as a novel cause of monogenic NS. Based on our findings, *NOS1AP* mutations impair the activation of the established actin regulator CDC42 and its effector DIAPH3. This leads to defective filopodia and podosome formation and decreased podocyte migration rate (PMR), resulting in aberrant glomerulogenesis in a human kidney organoid model and proteinuric kidney disease in mice. Established knowledge is listed on the left, while novel NS pathway steps based on our findings are on the right. Proteins encoded by human or mouse monogenic NS genes are encoded accordingly. Abbreviations: NS, nephrotic syndrome; PMR, podocyte migration rate.

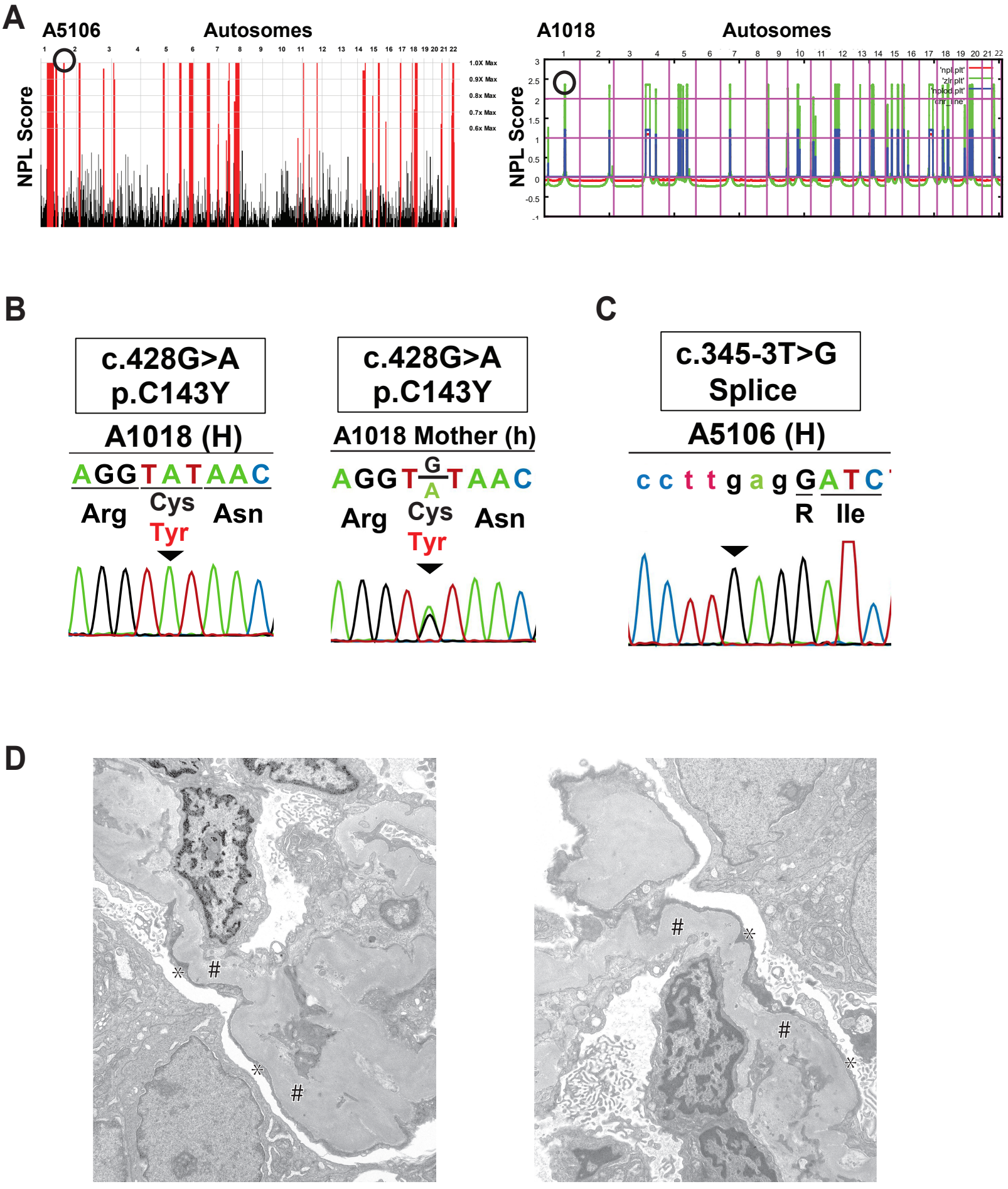
A
A5106
Autosomes
NPL Score
1.0X Max
0.9X Max
0.8x Max
0.7x Max
0.6x Max
A1018
Autosomes
NPL Score
'npl.plt'
'zlr.plt'
'nploid.plt'
'chr_line'
B
c.428G>A
p.C143Y
A1018 (H)
AGGTATAAC
Arg
Cys
Tyr
Asn
c.428G>A
p.C143Y
A1018 Mother (h)
AGGTG/ATAAC
Arg
Cys
Tyr
Asn
C
c.345-3T>G
Splice
A5106 (H)
cctt gag GATC
R
Ile
D

Figure S2. Sanger sequence confirms *NOS1AP* mutations in A1018 and A5106.

A. Homozygosity mapping identified recessive candidate loci. Profiles of nonparametric lod (NPL) scores across genome were generated based on WES variant data using Homozygosity Mapper for A5106 (left) and based on homozygous SNPs for A1018 (right). Maximum NPL peaks indicate candidate regions of homozygosity by descent as recessive candidate loci. Black circles demonstrate the peak regions in which *NOS1AP* variants were identified in chromosome 1.

B. Sanger tracings for affected subject A1018 (left) and his mother (right) are shown, which confirm the *NOS1AP* mutation c.428G>A and demonstrate maternal segregation.

C. Sanger tracings for affected subject A5106 confirms the homozygous splice variant in *NOS1AP*.

D. 2nd biopsy of patient A1018 was performed at 6 years of age. Micrographs prepared from the obtained tissue demonstrate flattened podocyte foot processes (asterisks) and thickened glomerular basement membrane (hashtags).

H, homozygous; h, heterozygous

A

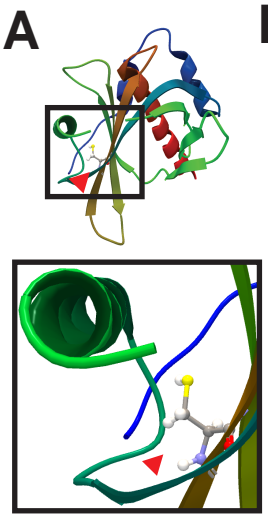

B

	NOS1AP PTB β-sheet 7 (AA position)								
	139	140	141	142	143	144	145	146	147
	N	I	F	R	C	N	V	F	K
H	9	17	16	0	0	79	0	0	0
K	0	6	0	11	0	0	0	0	11
R	11	22	6	3	0	0	0	0	14
D	0	6	0	1	0	0	0	0	2
E	7	10	0	4	0	0	0	0	8
N	16	0	11	0	0	1	0	0	0
Q	13	16	0	6	0	0	0	0	8
S	13	10	3	2	0	0	0	0	6
T	6	0	1	0	0	0	0	0	12
A	6	0	0	20	0	2	12	0	11
F	3	0	34	3	0	0	0	87	0
I	0	3	0	14	6	0	6	7	0
L	1	2	13	3	2	0	12	6	4
M	0	9	6	0	0	0	6	0	5
V	0	0	0	14	0	0	59	0	7
W	5	0	6	0	0	1	0	0	10
Y	3	0	4	14	0	11	0	1	1
C	2	0	0	6	86	0	6	0	2
G	0	0	0	0	0	0	0	0	0
P	0	0	1	0	0	0	0	0	0
Blank	6	0	0	0	7	7	0	0	0
Total	101	101	101	101	101	101	101	101	101

Amino Acid Frequency

C

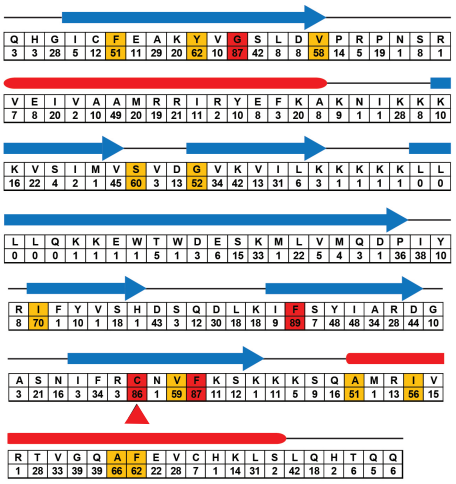

D

	3SO6	3F0W	2M38	1WJ1	5NJJ
3SO6		96	95	100	100
3F0W	1.123		84	112	117
2M38	1.401	1.403		84	90
1WJ1	1.327	0.807	1.730		112
5NJJ	1.078				

E

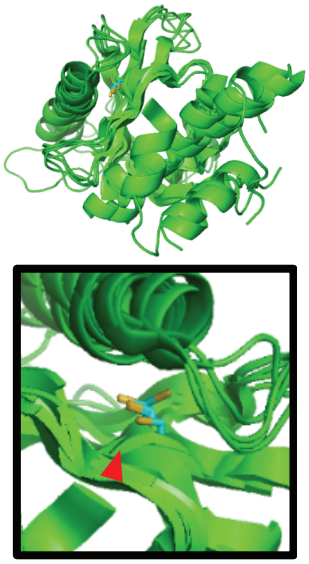

F

	3SO6	3F0W	2M38	1WJ1	5NJJ
Residue number	142	171	119	119	141
pseudo ΔΔG	-0.97	-1.14	-1.43	-1.39	-1.15

G

```
3so6A    042 ------------------------------------MEGMVFSLKYLGMTLVERPKGEELSAAAVKRIV 074
3f0wA    037 MHHHHHHSSGVDLGTENLYFQSMASR-PHQWQADEDAVRKGTCSFPVRYLGHVEVEESRGMHVCEDAVKKLK 107
2m38A    001 ------------------------STPVQAWQHHPEKLIAQSCDYKAAYLGSMLIKELRGTESTQDACAKMR 048
1wj1A    001 -------------GS---SGSSGASR-PHQWQTDEEGVRTGKCSFPVKYLGHVEVDESRGMHICEDAVKRLK 055
5njjA    020 ------------------------SR-PHQWQTDEEGVRTGKCSFPVKYLGHVEVDESRGMHICEDAVKRLK 066
NOS1AP   016 ------------------------LRI---PLHNEDAFQHGI-CFEAKYVGSLDVPRPNSRVEIVAAMRRIR 059

3so6A    075 ATAK-------AS---GKKLQKVTLKVSPRGIILTDSLTSQL----------------IENVSIYRISYCTA 120
3f0wA    108 A----------M---GRKSVKSVLWVSADGLRVVDDKTKDL----------------LVDQTIEKVSFCAP 149
2m38A    049 ANCQ-------KSTEQMKKVPTIILSVSAKGVKFIDATNKNI----------------IAEHEIRNISCAAQ 097
1wj1A    056 A----------T---GKKAVKAVLWVSADGLRVVDEKTKDL----------------IVDQTIEKVSFCAP 097
5njjA    067 AERKFFKGFFGKT---GKKAVKAVLWVSADGLRVVDEKTKDL----------------IVDQTIEKVSFCAP 119
NOS1AP   060 YEFK-------AK---NIKKKKVSIMVSVDGVKVILKKKKKLLLLQKKEWTWDESKMLVMQDPIYRIFYVSH 121

3so6A    121 DKMHDKVFAYIAQSQQNESLECHAFLCTKRKVAQAVTLTVAQAFKVAFEFWQVSLVPR-- 178
3f0wA    150 DRNLDKAFSYICRDGTTRRWICHCFLALK-DSGERLSHAVGCAFAACLERKQRREK---- 204
2m38A    098 DPEDLSTFAYITKDLKSNHHYCHVFTAFDVNLAAEIILTLGQAFEVAYQLALQARK---- 153
1wj1A    098 DRNFDRAFSYICRDGTTRRWICHCFMAVK-DTGERLSHAVGCAFAACLERKQKRSGPSSG 156
5njjA    120 DRNFDRAFSYICRDGTTRRWICHCFMAVK-DTGERLSHAVGCAFAACLERKQKREK---E 175
NOS1AP   122 DSQDLKIFSYIARDGASNIFRCNVFKSKKKSQAMRIVRTVGQAFEVCHKLSL---Q---- 174
```

H

Model	Overview	Zoomed red area
3F0W	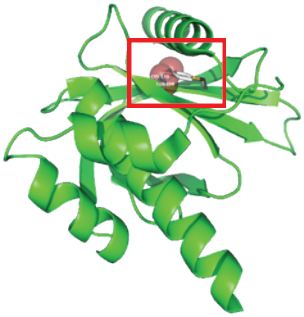	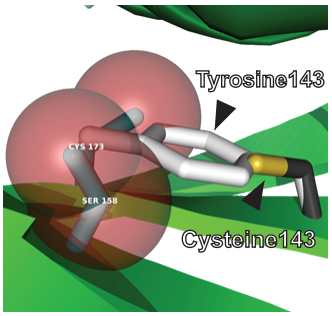
3SO6	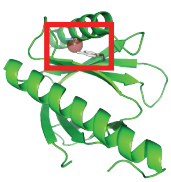	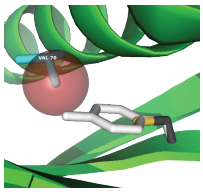
1WJ1	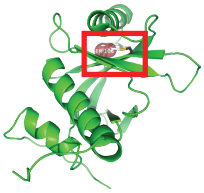	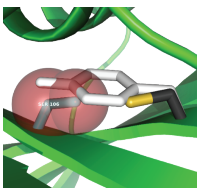
2M38	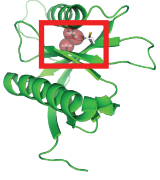	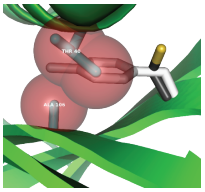
5NJJ	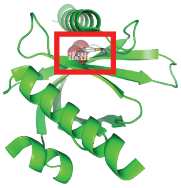	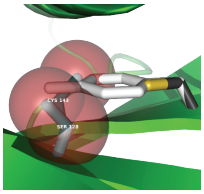

Figure S3. Paralog analysis reveals strong conservation of cysteine 143 in phosphotyrosine binding (PTB) domains and structural modeling of Cys143Tyr mutation predicts instability.

A. Ribbon structure of NUMB PTB domain (top) shows Cysteine 122 (red arrow), which is paralogous to NOS1AP cysteine 143. This cysteine residue is present on β-pleated sheet 7 in the NUMB PTB domain. A higher magnification image of the ball-and-stick representation is shown (bottom).
B. Frequency diagram of the primary amino acid sequence of 7th NOS1AP β-pleated sheet is shown. The absolute frequency of amino acids is shown below each NOS1AP residue. Cysteine 143 (red arrow) is conserved in 86/101 (85%) of PTB domains. Red shading indicates conservation in >75% PTB domains. Orange highlighting indicates conservation across 50-75% of PTB domains.
C. Frequency diagram shows the conservation of each amino acid in the NOS1AP PTB domain across 101 other PTB domains by multiple sequence alignment. Blue arrows indicate β-pleated sheets, while red bars denote α-helices. Cysteine 143 (red arrow) is only one of 4 amino acids in the 152 amino acid NOS1AP PTB domain that is highly conserved in >75% of PTB domains.
D. Matrix displays 5 structures (designated by protein data bank identifier) with from Psi-Blast search with >30% similarity to NOS1AP PTB sequence. The bottom left part of the table shows root-mean-square deviation, while the top right part indicates the number of residues aligned using PyMol.
E. Ribbon representation of the overlapping structures from (D) shows that these structures have high three-dimensional similarity and that the paralogous cysteines (stick representation) to NOS1AP cysteine 143 (**red** arrow) have similar localization in the paralogous structures.
F. The stability score output from Site Directed Mutator (pseudo ΔΔG) is shown. The negative values yielded for the cysteine-to-tyrosine mutation across all 5 structures suggests this mutation destabilizes the protein tertiary structure.
G. Expresso amino acid alignment is shown of structures from (D) to NOS1AP PTB domain. Cys143 and paralogous cysteines are colored in **red**. All residues that have at least one atom (excluding hydrogens) 5Å maximum away from the C_b or S_g atoms of the aligned cysteine are in yellow.
H. PyMol ribbon structures of paralogous PTB domain structural models are shown. In each structure, the mutated tyrosine residue (grey stick representation) clashes with neighboring amino acid residues (red spheres) relative to the wildtype cysteine residue (black/gold stick representation).

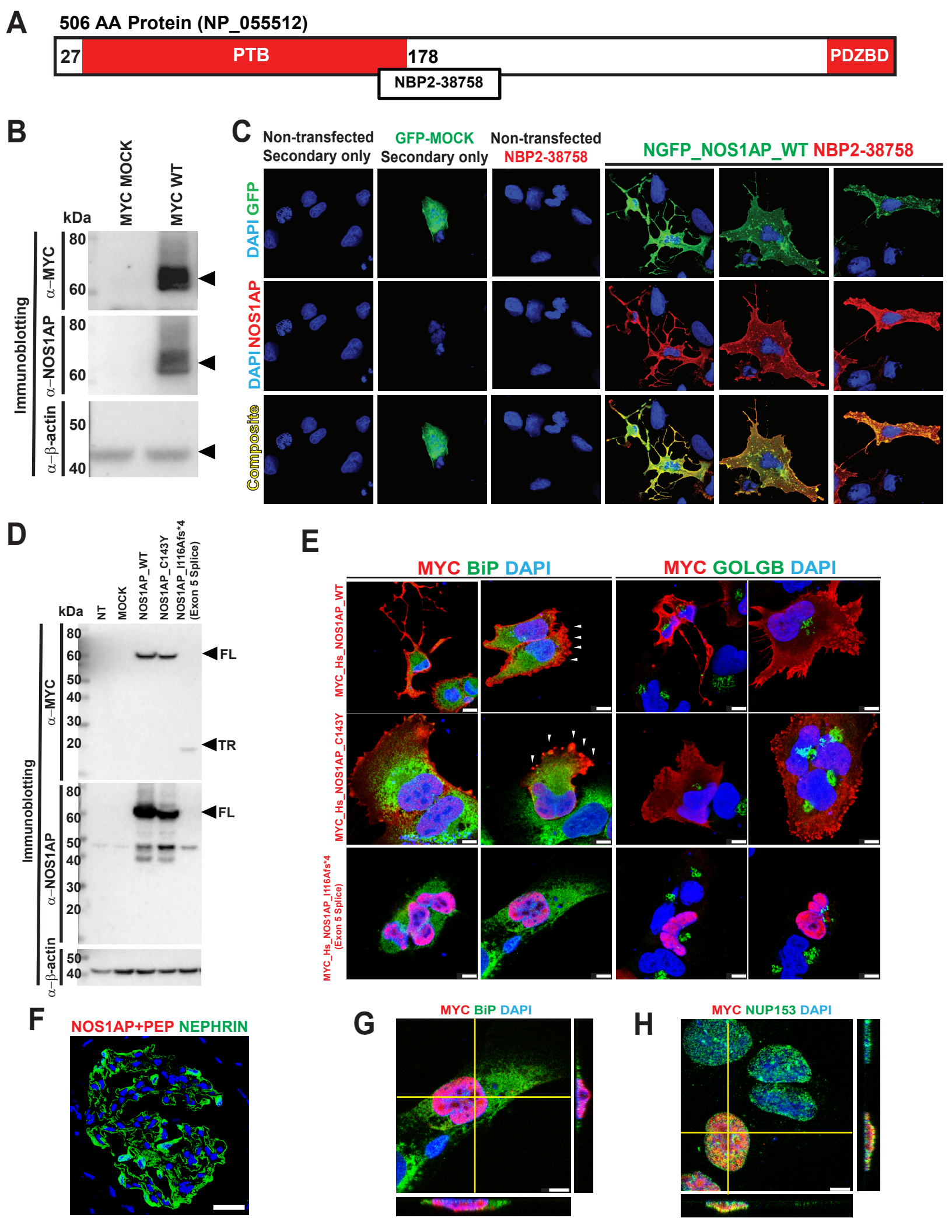
A
506 AA Protein (NP_055512)
27
PTB
178
PDZBD
NBP2-38758
B
MYC MOCK
MYC WT
kDa
Immunoblotting
α–MYC
α–NOS1AP
α–β-actin
80
60
50
40
C
Non-transfected
Secondary only
GFP-MOCK
Secondary only
Non-transfected
NBP2-38758
NGFP_NOS1AP_WT NBP2-38758
DAPI GFP
DAPI NOS1AP
Composite
D
kDa
NT
MOCK
NOS1AP_WT
NOS1AP_C143Y
NOS1AP_I116Afs*4 (Exon 5 Splice)
FL
TR
FL
E
MYC BiP DAPI
MYC GOLGB DAPI
MYC_Hs_NOS1AP_WT
MYC_Hs_NOS1AP_C143Y
MYC_Hs_NOS1AP_I116Afs*4 (Exon 5 Splice)
F
NOS1AP+PEP NEPHRIN
G
MYC BiP DAPI
H
MYC NUP153 DAPI

Figure S4. NOS1AP antibody validation effect of *NOS1AP* NS mutations (p.C143Y, p.I116Afs*4) on protein overexpression and localization in a human podocyte cell line.

A. NOS1AP protein domain structure is shown in relation to the immunogen against which the polyclonal rabbit NOS1AP antibody NBP2-38758 was generated.
B. Immunoblot shows that NBP2-38758 identifies overexpressed myc-tagged NOS1AP in a human podocyte cell line at the same molecular weight (kDa) as anti-myc antibody. β-actin levels demonstrate equivalent protein loading.
C. Co-immunofluorescence with NBP2-38758 reveals that this antibody identifies GFP-tagged NOS1AP upon overexpression in a human podocyte cell line (right 3 columns) by overlapping staining (yellow/orange overlap in composite row). Secondary only and non-transfected cell controls show no background signal.
D. Western blotting of Myc-tagged wild-type (WT) and NS mutation containing *NOS1AP* constructs expressed in a podocyte cell line shows comparable expression of WT and C143Y mutant at the full length size (FL), while the I116Afs*4 mutant yields a smaller protein at the expected 15 kDa size of the truncated protein (TR). Blots were interrogated with antibodies against MYC, NOS1AP and β-actin.
E. Upon overexpression of wildtype and NS mutant *NOS1AP* constructs, immunofluorescence and confocal microscopy imaging was performed with the ER marker BiP and the Golgi marker GOLGB. No constructs co-localize with BiP or GOLGB. WT and C143Y mutants similarly localize to cytoplasm and podosomes (arrowheads). The I116Afs*4 mutant construct co-localizes with DAPI staining in nucleus.
F. Immunofluorescence and confocal microscopy imaging of rat kidney sections demonstrates NOS1AP signal was abrogated by blocking peptide preadsorption (NOS1AP+PEP). Glomerular podocyte slit diaphragm marker nephrin co-staining was performed. Scale bar: 25 μm.
G. By immunofluorescence and confocal microscopy, Z-stack confirmed as in (E) that MYC-tagged NOS1AP I116Afs*4 mutant does not co-localize with the ER marker BiP.
H. Immunofluorescence and confocal microscopy was performed as in (E). Z-stack shows that the MYC-tagged NOS1AP I116Afs*4 mutant co-localizes to DAPI stained nuclei encircled by the NUP153 nuclear pore protein.

Abbreviations: FL, full-length NOS1AP; TR, truncated NOS1AP. (Scale bar: 7.5 μm)

A

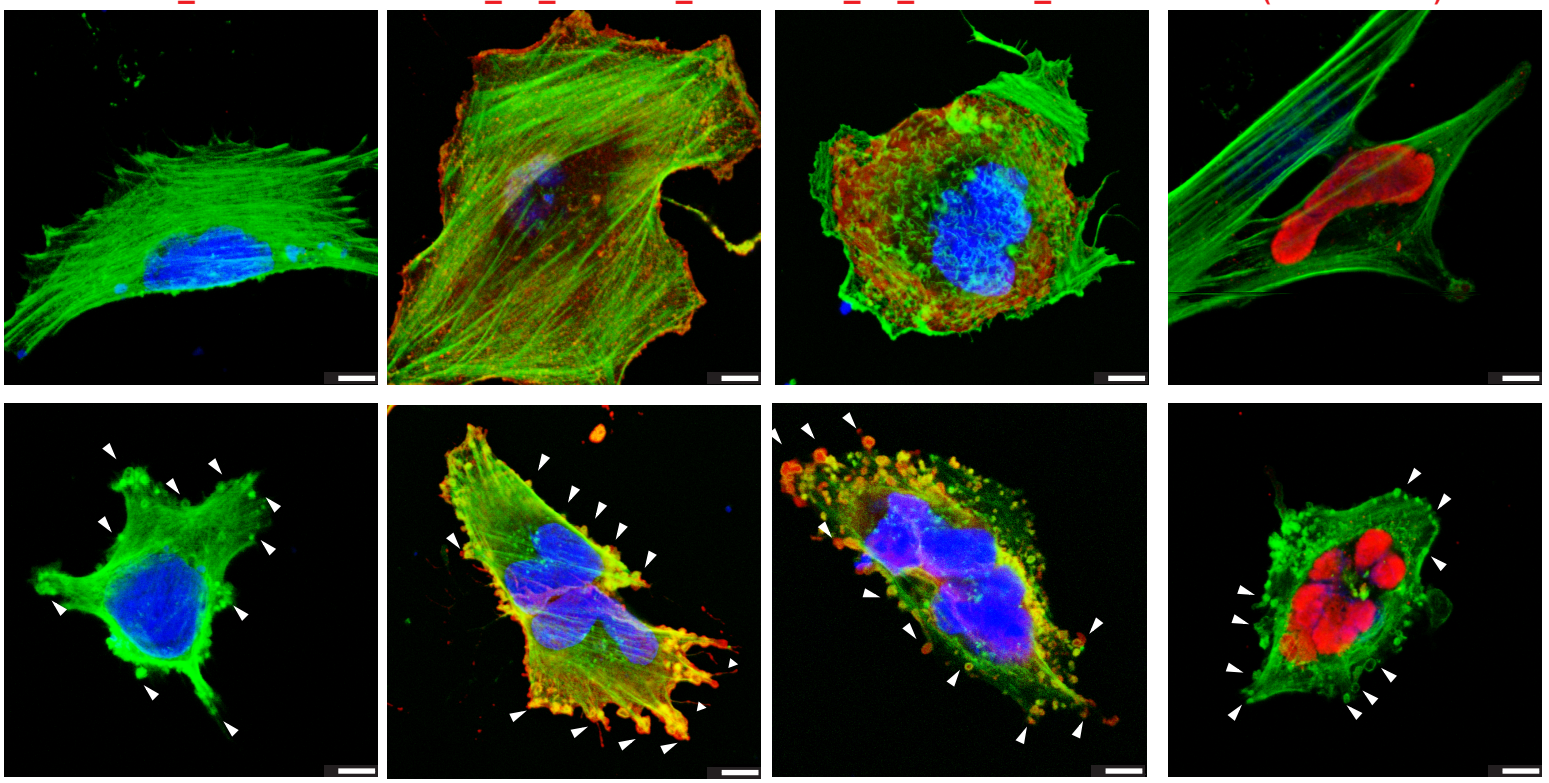

B

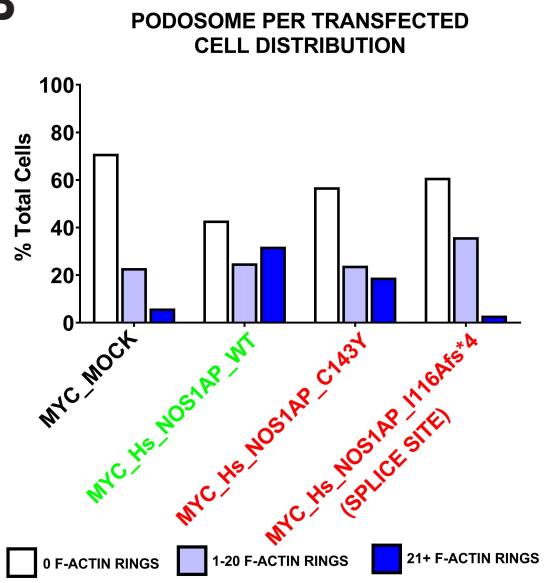

C

	% OF MYC(+) TRANSFECTED CELLS (N = 100 cells)			
F-actin(+) Podosomes per Cell	MYC_ MOCK	MYC_ NOS1AP_ WT	MYC_ NOS1AP_ C143Y	MYC_ NOS1AP_ I116A*fs4
0	71	43	57	61
1-10	12	13	13	26
11-20	11	12	11	10
21+	6	32	19	3

D

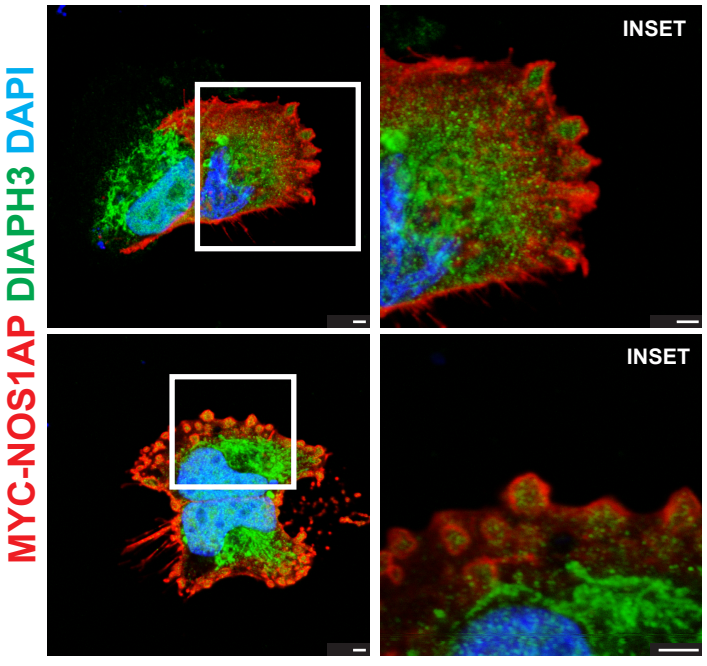

Figure S5. Wild-type *NOS1AP* increases podosome frequency and surrounds endogenous CDC42 effector DIAPH3 in podocytes, whereas human *NOS1AP* NS patient mutations have reduced effect

A. Human immortalized podocytes were transfected with MYC MOCK, MYC-tagged wildtype *NOS1AP* or NS mutants. Using immunofluorescence and confocal microscopy imaging, transfected cells (N = 100 cells per group) were scored for number of podosomes, defined as F-actin(+) peripheral rings. Representative images of cells from each transfection group are shown with podosomes indicated by white arrows. (Scale bar: 7.5 μm)

B. While only 6% of MOCK transfected cells had >21 podosomes, wildtype *NOS1AP* overexpression led 32% of cells with >21 podosomes. In contrast, the two mutant constructs p.C143Y and p.I116Afs*4 induced only 19% and 3% of cells with >21 podosomes, respectively.

C. Table shows scoring results from (B) by transfection group and cells with number of podosomes. There is a higher frequency of wild-type NOS1AP transfected cells with >21 podosomes when compared to the other transfected groups, as described in (A) (red outline).

D. Overexpressed MYC-NOS1AP (red) localizes to podosomes (based on NWASP localization in **Fig. 2D**) in a human podocyte cell line, in which the actin regulatory factor and CDC42 effector DIAPH3 (green) is present at the center of podosomes. (Scale bar: 2.5 μm)

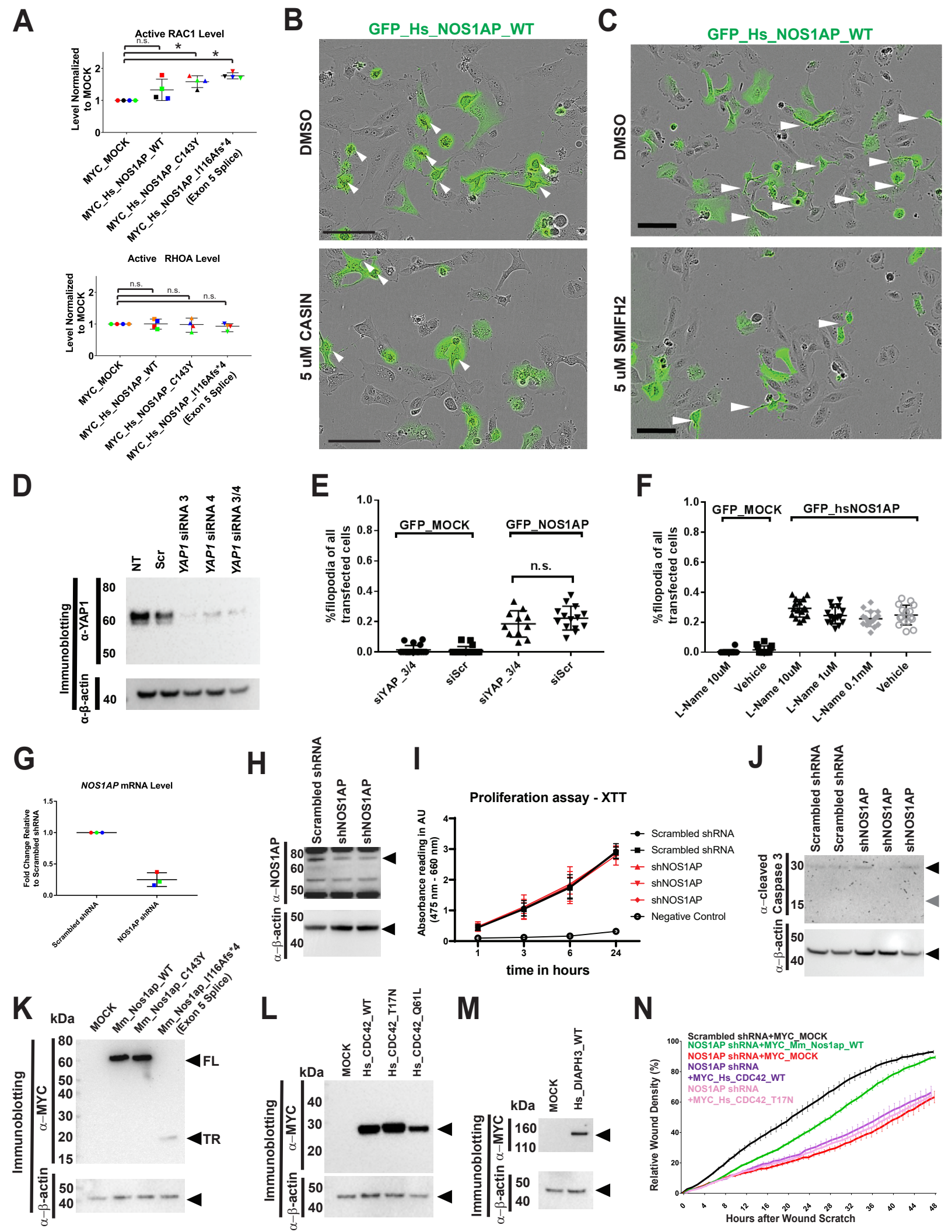
A
Active RAC1 Level
Level Normalized to MOCK
n.s.
*
*
MYC_MOCK
MYC_Hs_NOS1AP_WT
MYC_Hs_NOS1AP_C143Y
MYC_Hs_NOS1AP_I116Afs*4 (Exon 5 Splice)
Active RHOA Level
n.s.
n.s.
n.s.
B
GFP_Hs_NOS1AP_WT
DMSO
5 uM CASIN
C
GFP_Hs_NOS1AP_WT
DMSO
5 uM SMIFH2
D
NT
Scr
YAP1 siRNA 3
YAP1 siRNA 4
YAP1 siRNA 3/4
Immunoblotting
α-YAP1
α-β-actin
80
60
50
40
E
%filopodia of all transfected cells
GFP_MOCK
GFP_NOS1AP
n.s.
siYAP_3/4
siScr
siYAP_3/4
siScr
F
%filopodia of all transfected cells
GFP_MOCK
GFP_hsNOS1AP
L-Name 10uM
Vehicle
L-Name 10uM
L-Name 1uM
L-Name 0.1mM
Vehicle
G
NOS1AP mRNA Level
Fold Change Relative to Scrambled shRNA
Scrambled shRNA
NOS1AP shRNA
H
Scrambled shRNA
shNOS1AP
shNOS1AP
α–NOS1AP
α–β-actin
80
60
50
50
40
I
Proliferation assay - XTT
Absorbance reading in AU (475 nm - 660 nm)
time in hours
Scrambled shRNA
Scrambled shRNA
shNOS1AP
shNOS1AP
shNOS1AP
Negative Control
J
Scrambled shRNA
Scrambled shRNA
shNOS1AP
shNOS1AP
shNOS1AP
α–cleaved Caspase 3
α–β-actin
30
15
50
40
K
kDa
MOCK
Mm_Nos1ap_WT
Mm_Nos1ap_C143Y
Mm_Nos1ap_I116Afs*4 (Exon 5 Splice)
Immunoblotting
α–MYC
α–β-actin
80
60
50
40
30
20
15
50
40
FL
TR
L
kDa
MOCK
Hs_CDC42_WT
Hs_CDC42_T17N
Hs_CDC42_Q61L
Immunoblotting
α–MYC
α–β-actin
40
30
20
50
40
M
kDa
MOCK
Hs_DIAPH3_WT
Immunoblotting
α–MYC
α–β-actin
160
110
50
40
N
Scrambled shRNA+MYC_MOCK
NOS1AP shRNA+MYC_Mm_Nos1ap_WT
NOS1AP shRNA+MYC_MOCK
NOS1AP shRNA +MYC_Hs_CDC42_WT
NOS1AP shRNA +MYC_Hs_CDC42_T17N
Relative Wound Density (%)
Hours after Wound Scratch

Figure S6. Effect of overexpressed NOS1AP on active RHOA and RAC1 levels and of pharmacological inhibition on NOS1AP induced filopodia formation, and *NOS1AP* knockdown and *Nos1ap*, *CDC42*, and *DIAPH3* cDNA rescue in human immortalized podocytes.

A. HEK293T cells were transfected as in **Figure 3C**. Active RAC1 levels were measured by G-LISA RAC1 assay. Wildtype NOS1AP did not significantly increase active RAC1 levels, while NS mutant constructs did (1.59 and 1.77-fold increases) (1-way ANOVA). Active RHOA levels were measured by G-LISA RHOA assay. Wildtype and mutant constructs had no significant effect on active RHOA levels (1-way ANOVA). Each dot represents an independent biological replicate.

B. A human podocyte cell line expressing MOCK-GFP or GFP tagged WT NOS1AP was treated with increasing doses of CDC42 inhibitor CASIN or the vehicle DMSO. Filopodia formation was quantified as in **Figure 3B** at 13 hours after transfection. Representative images for **Figure 3D** are shown with white arrows pointing to cells bearing ≥2 filopodia (scale bar: 100 μM).

C. A human podocyte cell line expressing MOCK GFP or GFP tagged WT NOS1AP was treated with increasing doses of formin inhibitor SMIFH2 or vehicle DMSO. Filopodia formation was quantified as in **Figure 3B** at 14 hours after transfection. Representative images for **Figure 3E** are shown with white arrows pointing to cells bearing filopodia (scale bar: 100 μM).

D. siRNA Knockdown of *YAP1* with two independent siRNA in a podocyte cell line was validated by western blot relative to non-transfected (NT) and scrambled siRNA transfected (Scr) controls.

E. Human immortalized podocyte cells were transfected with either scrambled or *YAP1* siRNA and, at 24 hours, with Mock-GFP or GFP tagged WT NOS1AP. Filopodia formation was quantified as in **Figure 3B** at 10 hours after plasmid transfection. There was no statistically significant difference in filopodia formation with *YAP1* knockdown by 1-way ANOVA.

F. As in (E), human podocytes transfected with either Mock-GFP or GFP tagged WT NOS1AP were subsequently treated with NOS1 inhibitor and arginine analog L-NAME versus vehicle control (PBS). Filopodia formation was quantified as in **Figure 3B** at 13 hours. There was no difference in NOS1AP-induced filopodia formation between L-NAME and vehicle groups.

G. Quantitative RT-PCR of *NOS1AP* mRNA expression was performed in scrambled shRNA expressing *versus NOS1AP*-specific shRNA expressing human immortalized podocytes. Mean *NOS1AP* knockdown was 75% relative to scrambled control cells.

H. Knockdown of NOS1AP was assessed by western blot, showing reduced protein expression in knockdown cells relative to scrambled control (black arrowhead).

I. Cell proliferation assay (XTT) was performed in human immortalized podocytes. Graph shows absorbance readings (475 nm – 660 nm) in arbitrary units for negative control (full media only), two independent scrambled shRNA control lines and three independent lines expressing *NOS1AP*-specific shRNA. No discernible difference in proliferation behavior was observed in between the different cell lines.

J. Immunoblotting for apoptosis marker cleaved caspase 3 was performed in scrambled shRNA expressing *versus NOS1AP*-specific shRNA expressing human immortalized podocytes. Long exposure (3000 s) reveals faint band at the size of (uncleaved) procaspase 3 (black arrowhead) but no detectable signal at the expected size of cleaved caspase 3 (grey arrowhead).

K. cDNA constructs of myc-tagged wildtype mouse *Nos1ap* (WT) and constructs based on human *NOS1AP* mutations (C143Y, I116Afs*4) were over-expressed in a *NOS1AP* shRNA expressing human podocyte cell line. Protein lysates at 12 hours post-transfection were evaluated by immunoblotting, showing comparable protein levels of the wildtype and C143Y construct (FL, full length). The I116Afs*4 construct has lower protein levels at a smaller molecular weight (TR, truncated).

L. As in (K), a *NOS1AP* shRNA podocyte cell line was transfected with cDNA of myc-tagged wildtype human *CDC42* (WT) and cDNA constructs of the hypomorphic variant T17N and constitutively active variant Q61L. Protein lysates at 24 hours post-transfection were evaluated by immunoblotting, showing comparable protein levels.

M. As in (K), a *NOS1AP* shRNA podocyte cell line was transfected with a myc-tagged wildtype human *DIAPH3* cDNA construct. Protein lysates at 24 hours post-transfection were evaluated by immunoblotting, showing expression of this construct.

N. Knockdown of *NOS1AP* (red) caused reduced PMR compared with scrambled shRNA (black). This was rescued by overexpression of WT *Nos1ap* (green) but not by wildtype *CDC42* (purple) nor the hypomorphic *CDC42* mutant T17N (pink).

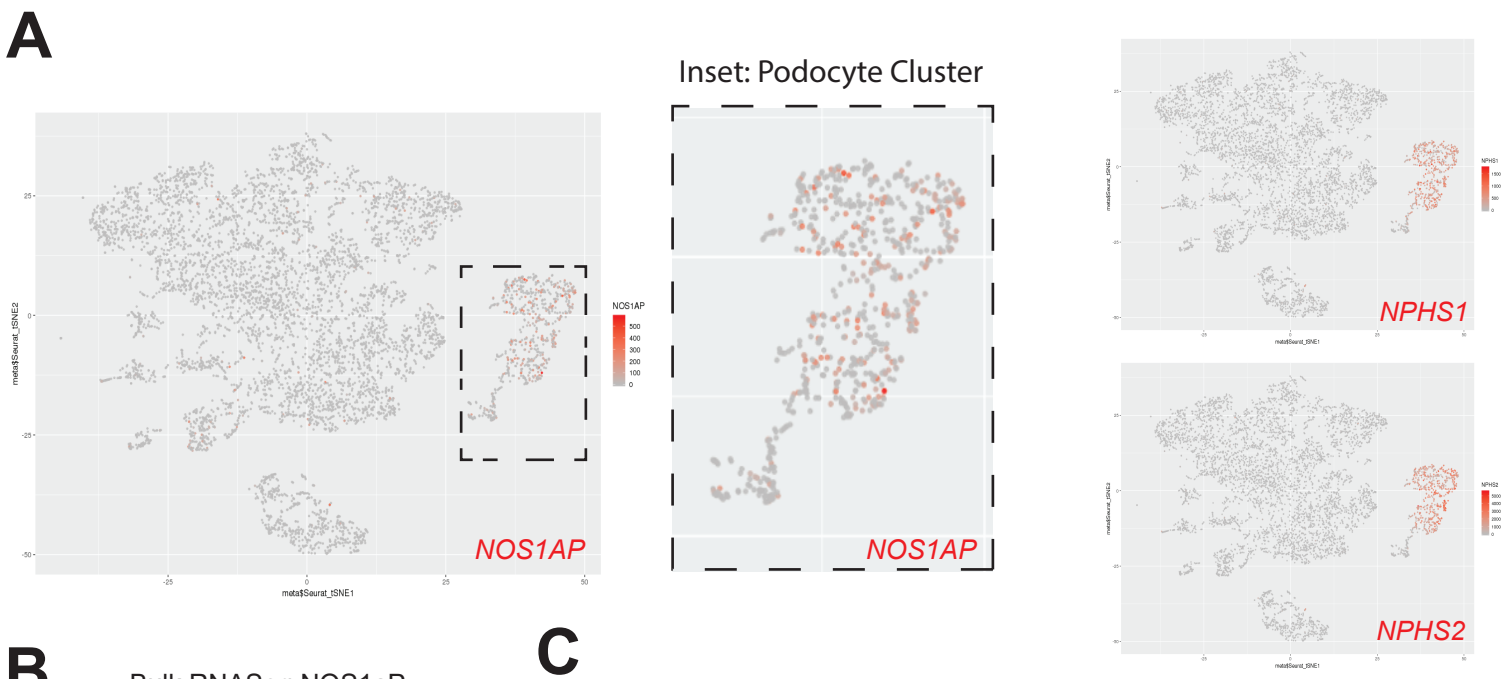
A
Inset: Podocyte Cluster
NOS1AP
NOS1AP
NPHS1
NPHS2

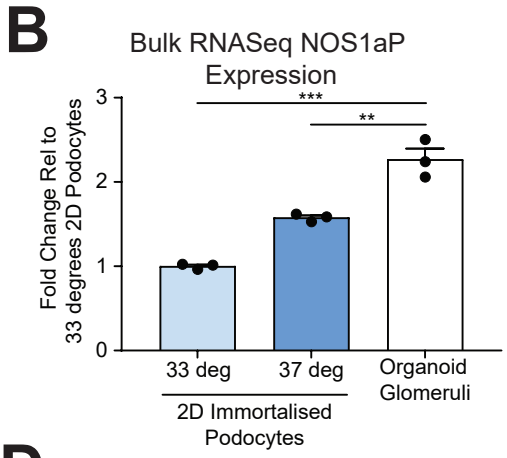
B
Bulk RNASeq NOS1aP Expression
Fold Change Rel to 33 degrees 2D Podocytes
***
**
33 deg
37 deg
Organoid Glomeruli
2D Immortalised Podocytes

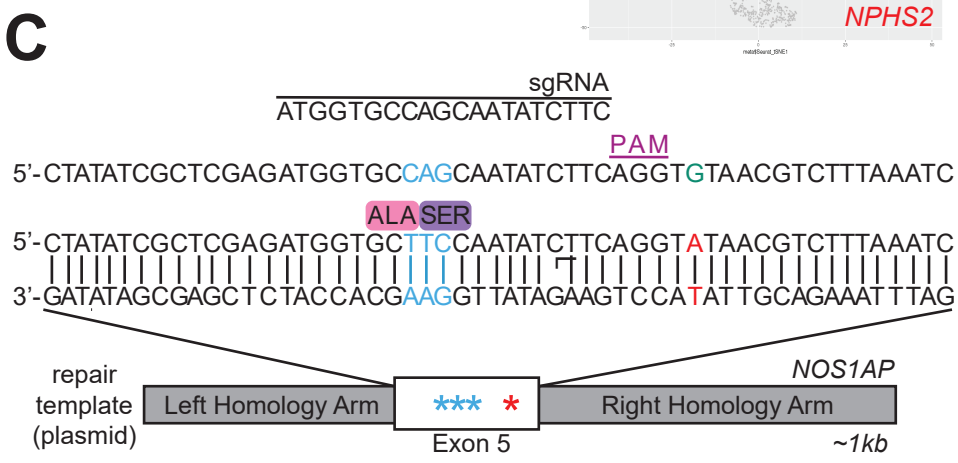
C
sgRNA
ATGGTGCCAGCAATATCTTC
PAM
5'-CTATATCGCTCGAGATGGTGCCAGCAATATCTTCAGGTGTAACGTCTTTAAATC
ALA SER
5'-CTATATCGCTCGAGATGGTGCTTCCAATATCTTCAGGTATAACGTCTTTAAATC
3'-GATATAGCGAGCTCTACCACGAAGGTTATAGAAGTCCATATTGCAGAAATTTAG
repair template (plasmid)
Left Homology Arm
Right Homology Arm
Exon 5
NOS1AP
~1kb

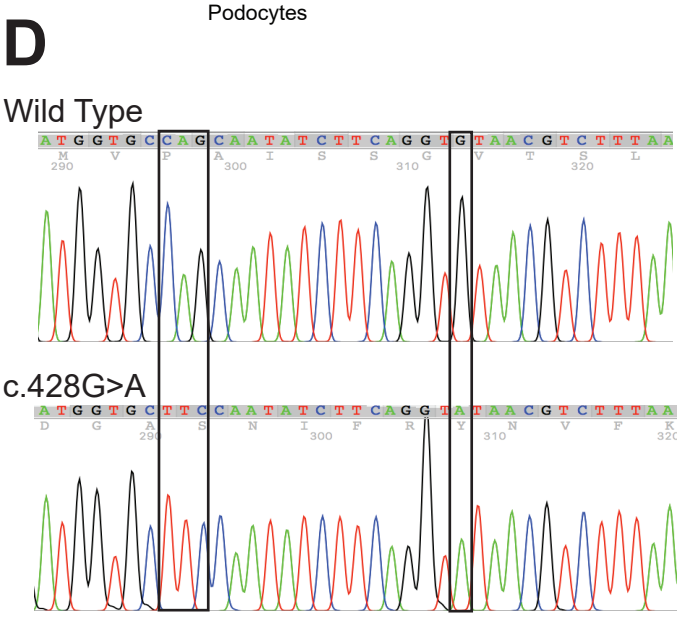
D
Wild Type
c.428G>A

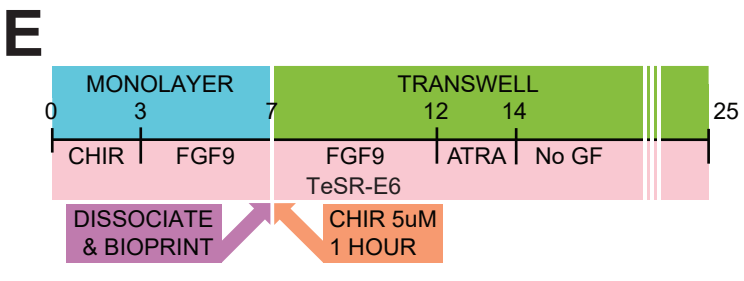
E
MONOLAYER
TRANSWELL
0
3
7
12
14
25
CHIR
FGF9
FGF9
TeSR-E6
ATRA
No GF
DISSOCIATE & BIOPRINT
CHIR 5uM 1 HOUR

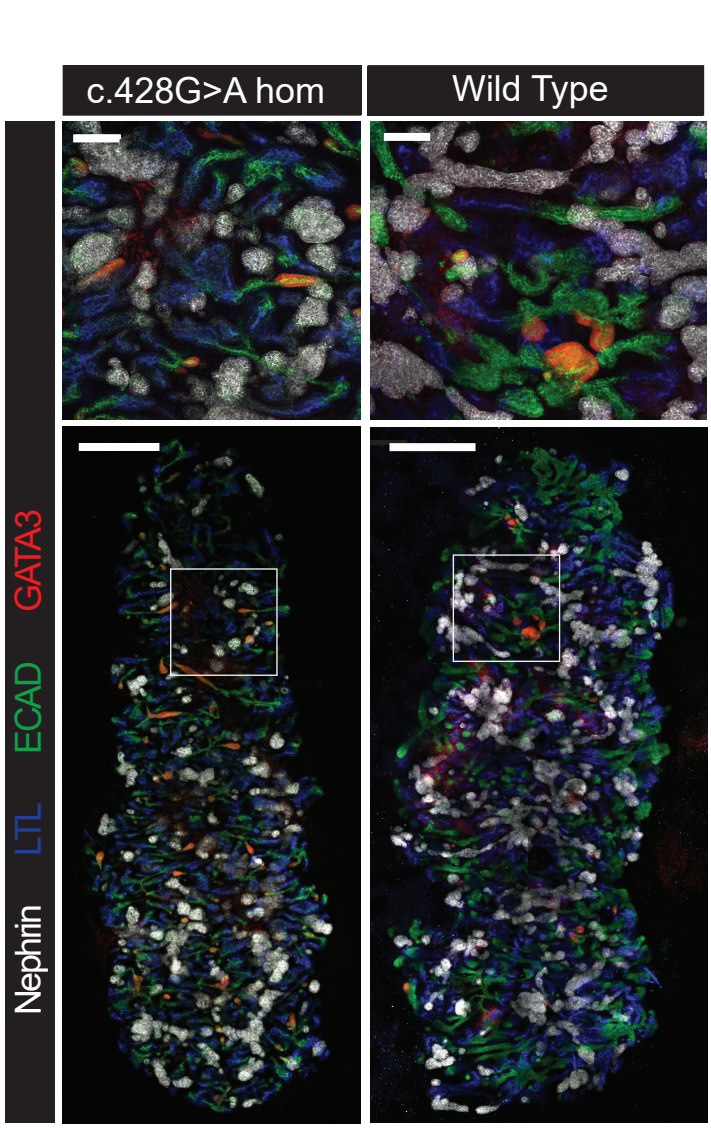
F
c.428G>A hom
Wild Type
GATA3
ECAD
LTL
Nephrin

Figure S7. Generation of human iPSC-derived and kidney organoids harboring the recessive *NOS1AP* NS patient mutation c.428G>A.

A. Single cell RNA sequencing data of wild type kidney organoids illustrates enrichment of *NOS1AP* mRNA expression in the podocyte cluster, which is marked by enriched expression of *NPHS1 and NPHS2*.
B. Bulk RNA sequencing data illustrates increased *NOS1AP* mRNA expression in sieved 3D organoid glomeruli than in 2D cultures of immortalized podocytes.
C. The CRISPR guide RNA and DNA repair template is shown, which was employed to mutate the wildtype (WT) G nucleotide (green) for missense variant A (red) for G. In addition, the synonymous 3bp change (blue) upstream was employed for ease of identification of edited clones.
D. Sanger sequencing chromatograms from WT and *NOS1AP* mutant (c.428G>A) iPSC clones are shown, demonstrating knock-in of the c.428G>A missense variant (red) and the synonymous 3bp change (blue) in the mutant clone.
E. Kidney organoid differentiation schema is shown. The organoid culture was performed as described before (62, 63). The following doses were employed for each reagent: CHIR99021 7um, FGF9 200ng/mL, and ATRA 2uM. No GF (growth factors) were administered after day 14.
F. Immunofluorescence images of bioprinted kidney organoids from both iPSC clones showing expected staining for podocytes (Nephrin in white), proximal tubule cells (LTL in blue), distal tubule cells (ECAD in green) and urothelial precursor cells (positive for both ECAD in green and GATA3 in red). (Low power scale bar 500 μm, inset scale bar 100 μm.)

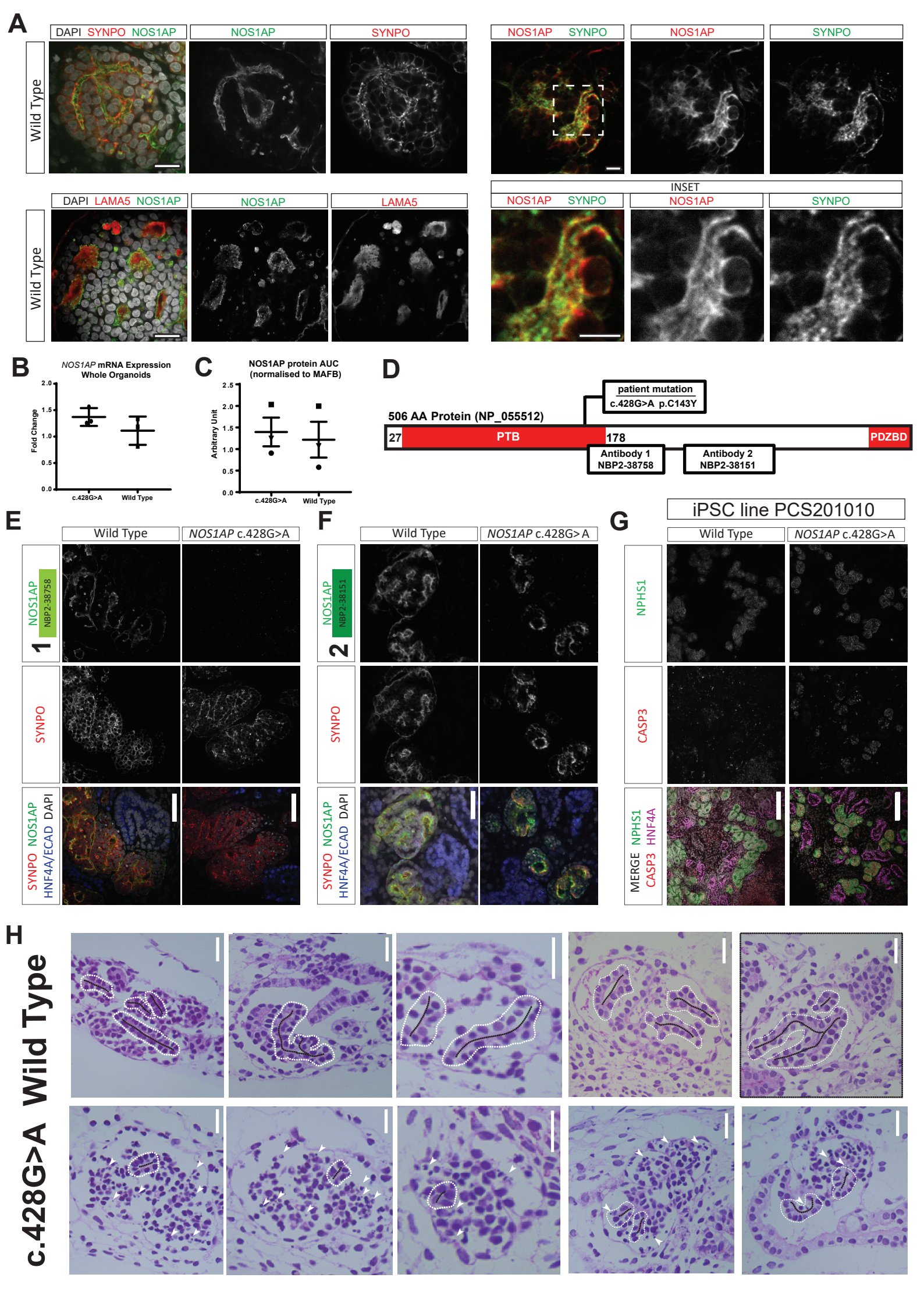
A
DAPI SYNPO NOS1AP
NOS1AP
SYNPO
NOS1AP SYNPO
NOS1AP
SYNPO
Wild Type
DAPI LAMA5 NOS1AP
NOS1AP
LAMA5
INSET
NOS1AP SYNPO
NOS1AP
SYNPO
Wild Type
B
NOS1AP mRNA Expression
Whole Organoids
Fold Change
c.428G>A
Wild Type
C
NOS1AP protein AUC
(normalised to MAFB)
Arbitrary Unit
c.428G>A
Wild Type
D
506 AA Protein (NP_055512)
patient mutation
c.428G>A p.C143Y
27
PTB
178
PDZBD
Antibody 1
NBP2-38758
Antibody 2
NBP2-38151
E
Wild Type
NOS1AP c.428G>A
1
NOS1AP
NBP2-38758
SYNPO
SYNPO NOS1AP
HNF4A/ECAD DAPI
F
Wild Type
NOS1AP c.428G>A
2
NOS1AP
NBP2-38151
SYNPO
SYNPO NOS1AP
HNF4A/ECAD DAPI
G
iPSC line PCS201010
Wild Type
NOS1AP c.428G>A
NPHS1
CASP3
MERGE NPHS1
CASP3 HNF4A
H
Wild Type
c.428G>A

Figure S8. Kidney organoids harboring the recessive *NOS1AP* NS patient mutation c.428G>A show comparable NOS1AP protein levels but exhibit aberrantly formed glomeruli and increased apoptosis.

A. Immunofluorescence of NOS1AP demonstrates localization to podocytes in organoid glomeruli adjacent to the podocyte marker synaptopodin (SYNPO; merge image shown in **Figure 4A**) and basement membrane protein laminin A5 (LAMA5). (Scale Bars left panel 20 μm, right panel 10 μm.)
B. Quantification of *NOS1AP* mRNA levels normalized to *MAFB* mRNA levels by quantitative RT-PCR shows no significant difference between wildtype and knock-in organoids.
C. Quantitation of NOS1AP protein levels normalized to MAFB protein levels by SimpleWes capillary Western Blot shows no significant difference between wildtype and knock-in organoids.
D. Schematic overview of human NOS1AP protein shows the position of patient A1018 missense mutation as well as the immunogens used to generate two different NOS1AP antibodies. Antibody 1, Novus NBP2-38758; Antibody 2, Novus NBP2-38151.
E. By whole-mount immunofluorescence staining with NOS1AP antibody 1, wild type organoids demonstrate NOS1AP localization to glomeruli (SYNPO) with no signal evident in proximal (HNF4A, nuclear) or distal (ECAD, cell wall) tubules. *NOS1AP* c.428G>A organoids demonstrated no detectable NOS1AP signal. (Scale bars: 50 μm). This was validated across multiple differentiations in two independent iPSC backgrounds.
F. Whole-mount immunofluorescence using NOS1AP antibody 2, which was generated against a more C-terminal immunogen of NOS1AP, shows comparable signal intensity and glomerular localization both for wild type and *NOS1AP* c.428G>A organoids.
G. Whole-mount immunofluorescence of organoids derived from iPSC cell line PCS201010 (iPSC cell line CRL1502 shown in **Figure 4F**) for apoptotic marker cleaved capase 3 (CASP3) is shown. CASP3 signal is increased in glomeruli (NPHS1 positive area) of *NOS1AP* mutant organoid glomeruli, relative to wildtype organoids. CASP3 signal in tubular segments (HNF4A positive area) is not increased. (Scale Bar 100 μm.)
H. Additional images of wildtype (WT) and *NOS1AP* c.428G>A mutant organoids (PAS staining) are shown as in **Figure 4B**, where glomerular tufts (within white lines) were defined as linear podocyte monolayers organized bilaterally about established extracellular matrix (black lines) and were reduced in *NOS1AP* mutant organoids. Mutant organoids also demonstrate increased pyknotic nuclei (arrowheads), indicative of cell death. (Scale Bar 20 μm.)

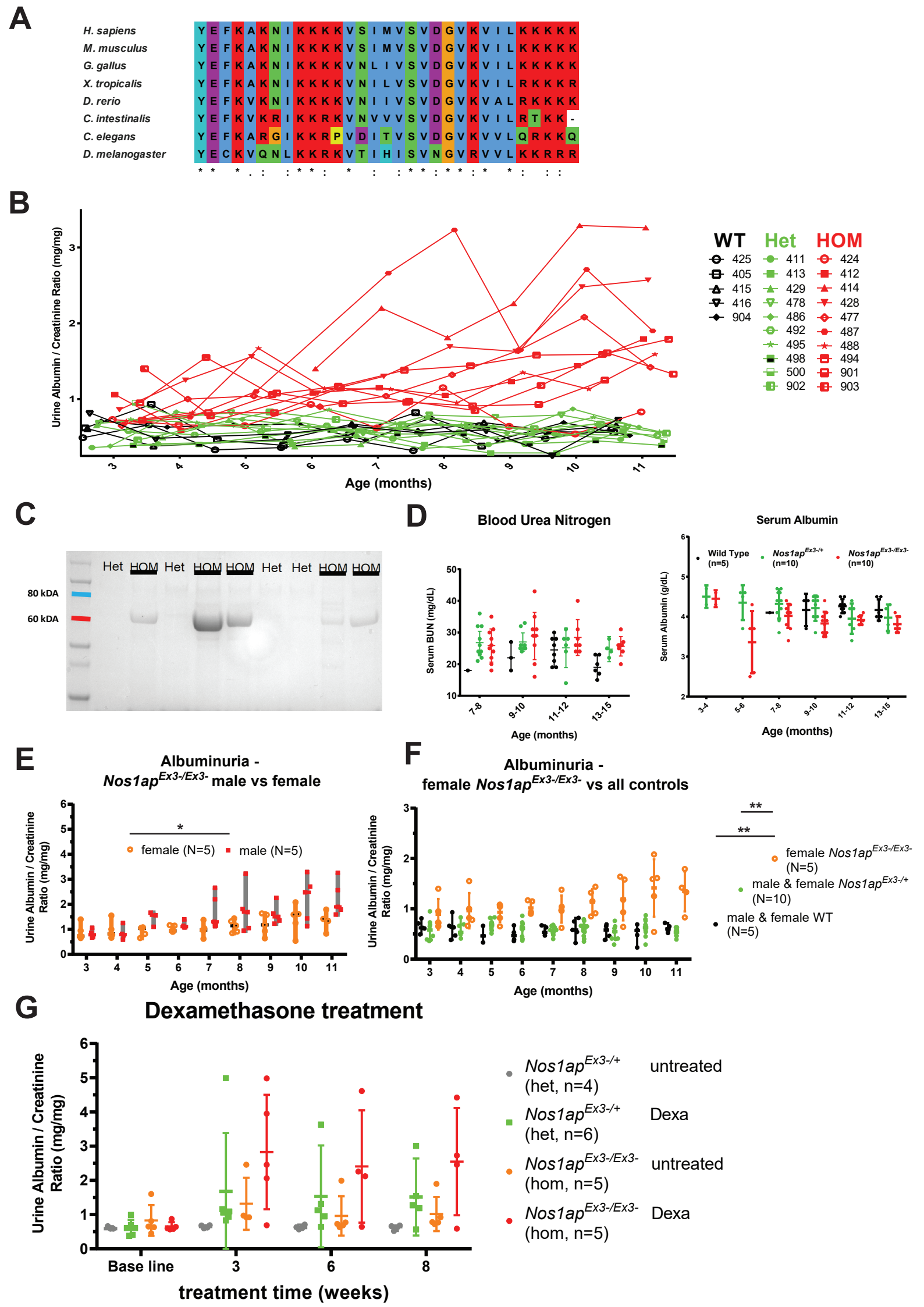
A
H. sapiens
M. musculus
G. gallus
X. tropicalis
D. rerio
C. intestinalis
C. elegans
D. melanogaster
B
Urine Albumin / Creatinine Ratio (mg/mg)
Age (months)
WT
Het
HOM
425
405
415
416
904
411
413
429
478
486
492
495
498
500
902
424
412
414
428
477
487
488
494
901
903
C
80 kDA
60 kDA
Het
HOM
D
Blood Urea Nitrogen
Serum BUN (mg/dL)
Age (months)
Serum Albumin
Wild Type (n=5)
Nos1ap Ex3-/+ (n=10)
Nos1ap Ex3-/Ex3- (n=10)
Serum Albumin (g/dL)
E
Albuminuria - Nos1ap Ex3-/Ex3- male vs female
female (N=5)
male (N=5)
F
Albuminuria - female Nos1ap Ex3-/Ex3- vs all controls
female Nos1ap Ex3-/Ex3- (N=5)
male & female Nos1ap Ex3-/+ (N=10)
male & female WT (N=5)
G
Dexamethasone treatment
Base line
treatment time (weeks)
Nos1ap Ex3-/+ (het, n=4) untreated
Nos1ap Ex3-/+ (het, n=6) Dexa
Nos1ap Ex3-/Ex3- (hom, n=5) untreated
Nos1ap Ex3-/Ex3- (hom, n=5) Dexa

Figure S9. *Nos1ap*$^{Ex3-/Ex3-}$ mice develop glomerular proteinuria but not hypoalbuminemia which is not ameliorated by dexamethasone treatment.

A. Amino acid sequence conservation of PTB region encoded by Nos1ap exon 3 shows 12/31 amino acids are identical from vertebrate to invertebrate species down to C. elegans.

B. Urinary albumin / creatinine ratios (3-11 months) for 5 wild type, 10 heterozygous *Nos1ap*$^{Ex3-/+}$ and 10 homozygous *Nos1ap*$^{Ex3-/Ex3-}$ mice are depicted. Each line represents an individual animal. *Nos1ap*$^{Ex3-/Ex3-}$ mice develop significant albuminuria across the displayed time-course.

C. Coomassie blue staining of acrylamide gel is shown, in which urine proteins are visualized from homozygous *Nos1ap*$^{Ex3-/Ex-}$ (HOM) and heterozygote mice (Het). ~60 kDA protein bands, consistent with albumin, are noted in homozygote urine but not heterozygote urine.

D. Blood urea nitrogen (BUN) levels and Serum albumin levels (7-15 months) for 5 wild type, 10 heterozygous Nos1ap$^{Ex3-/+}$ and 10 homozygous Nos1ap$^{Ex3-/Ex3-}$ mice are depicted. Nos1ap$^{Ex3-/Ex3-}$ mice developed significant albuminuria **(Figure 5B, S19A)** but no renal failure or significant hypoalbuminemia as indicated by normal-range BUN levels or serum albumin levels respectively across the displayed time-course.

E. Urinary albumin / creatinine ratios (3-11 months) for 5 male and 5 female homozygote *Nos1ap*$^{Ex3-/Ex3-}$ mice are depicted. Male mice exhibit more albuminuria than females. Wilcoxon test, *p<0.05.

F. Urinary albumin / creatinine ratios (3-11 months) for 5 wild type, 10 heterozygous *Nos1ap*$^{Ex3-/+}$ and 5 female homozygous *Nos1ap*$^{Ex3-/Ex3-}$ mice are depicted. Female *Nos1ap*$^{Ex3-/Ex3-}$ mice develop significant albuminuria when compared to control male and female mice. Friedman test, **p<0.01.

G. Urinary albumin / creatinine ratios (3-5 months) for heterozygous *Nos1ap*$^{Ex3-/+}$ and homozygous *Nos1ap*$^{Ex3-/Ex3-}$ mice treated with dexamethasone (Dexa) or vehicle (untreated) are depicted. Dexamethasone increases albuminuria in both heterozygotes and homozygotes.

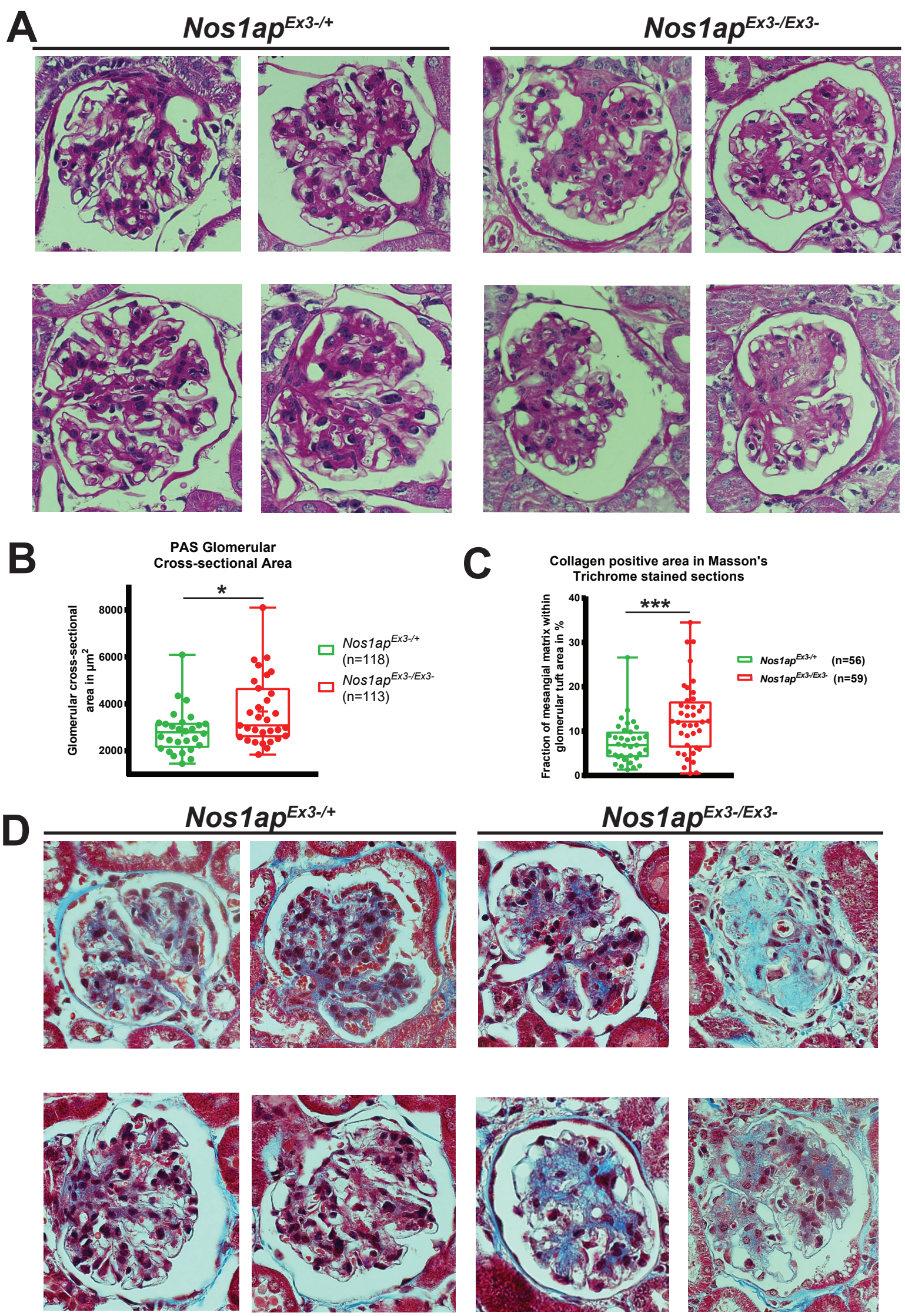
A
Nos1ap Ex3-/+
Nos1ap Ex3-/Ex3-
B
PAS Glomerular
Cross-sectional Area
Glomerular cross-sectional area in µm2
8000
6000
4000
2000
*
Nos1ap Ex3-/+ (n=118)
Nos1ap Ex3-/Ex3- (n=113)
C
Collagen positive area in Masson's Trichrome stained sections
Fraction of mesangial matrix within glomerular tuft area in %
40
30
20
10
0
***
Nos1ap Ex3-/+ (n=56)
Nos1ap Ex3-/Ex3- (n=59)
D
Nos1ap Ex3-/+
Nos1ap Ex3-/Ex3-

Figure S10. *Nos1ap*$^{Ex3-/Ex3-}$ mice exhibit increased mesangial expansion, glomerular size, and glomerular sclerosis.

A. (A) Representative PAS stained kidney sections for *Nos1ap*$^{Ex3-/+}$ and *Nos1ap*$^{Ex3-/Ex3-}$ mice are shown (5 animals per genotype, 11 months old (3) and 16 months old (2)) (Scale Bar: 200 μm). Homozygote mice have increased matrix expansion and glomerular size.
B. (B) Box Plot shows glomerular cross-sectional area (each dot represents one glomerulus from animals in (A)). Mann-Whitney test, *p<0.05.
C. (C) Box Plot shows fraction of collagen deposition in glomeruli based on Masson's Trichrome staining in (D) (each dot represents one glomerulus from animals as in (A)). Kruskal-Wallis test, ***p<0.001
D. (D) Representative Masson's Trichrome stained kidney sections for *Nos1ap*$^{Ex3-/+}$ and *Nos1ap*$^{Ex3-/Ex3-}$ mice are shown (animal numbers as in (A), Scale Bar: 200 μm). Homozygote mice have increased sclerosis.